Rare Earth Oxide Coating of the Walls of SBA-15

J. Sauer, F. Marlow, B. Spliethoff, and F. Schüth*

Max-Planck-Institut für Kohlenforschung, Kaiser Wilhelm Platz 1, 45470 Mülheim, Germany

Received May 23, 2001. Revised Manuscript Received September 3, 2001

Rare earth oxide dispersions, primarily europium doped yttria (YOX), in the ordered mesoporous material SBA-15 were synthesized by impregnating the calcined host material with different aqueous rare earth nitrate solutions and subsequent calcination. The materials obtained were characterized by N_2-sorption measurements, XRD, TEM, IR, and optical spectra. The data suggest a coating of the internal surfaces of SBA-15 by rare earth oxides at loadings up to a monolayer, while at higher loading oxide nanoparticles form.

Introduction

Oxide dispersions in ordered mesoporous materials have attracted growing attention in the last years. The first work in this field, published in 1995, was dealing with the incorporation of Fe_2O_3 particles in MCM-41.[1,2] The impregnation of MCM-41 with aqueous solutions of $Fe(NO_3)_3$, drying, and calcination led to the formation of Fe_2O_3 particles in the host material. While in these initial papers the preparation and characterization of oxide dispersions was the focus of attention, subsequently iron oxide loaded mesoporous materials were found to be superior to conventional iron oxide-on-silica catalysts in the oxidation of SO_2 to SO_3.[3] Also, MCM-48, which has a three-dimensional pore system as compared to the unidimensional system of MCM-41, was used for the synthesis of iron oxide dispersions. These materials were investigated in much detail with respect to the state of the iron.[4]

Other metal oxides have been supported on ordered mesoporous silica as well. The best way to classify these materials is the mode of preparation. The most common method up to now seems to be impregnation with solutions of thermally unstable precursor salts. After drying and calcination, oxide particles are formed in the host structure. This method was used, for instance, to obtain cesium oxide particles,[5] Ga_2O_3 and In_2O_3 particles,[6] and Cu_2O particles[7] in MCM-41. The formation of the mixed oxide $CsLaO_2$ and its behavior as a basic solid-state catalyst were studied in ref 8.

The second method applied in the synthesis of oxide dispersions is the use of organic metal precursors, which react as bases and can thus be grafted on the surface of the silica. In contact with the siliceous host material, the surface of which is covered with acidic silanol groups, the protons of the silanol groups are substituted by a part of the organic metal precursor. This grafting procedure typically results in molecularly dispersed species after the grafting step, but calcination often leads to formation of oxide particles in the pore system of the host material. Though the dispersion of the metal oxide is usually high and mainly determined by the area density of silanol groups, the disadvantage of this method is, in comparison with the former one, that often only lower loadings are achieved, even if there are exceptions to this general trend.[9] Moreover, grafting procedures typically involve more complex and expensive precursor species.

This method was applied among others for the synthesis of titania in MCM-41[10] and zirconia in MCM-48.[11] In the former case $Ti(OBut)_4$ and in the latter case $Zr(OPr)_4$ were used as basic reagents for grafting onto the silica surface. Also, several rare earth complexes have been grafted on the surface of ordered mesoporous silicas by Anwander and co-workers,[12−16] although here the incorporation of the intact complex and not an oxide was the center of attention.

Other methods used are the solid-state exchange and the loading via the gas phase by a volatile precursor and subsequent calcination. Solid-state exchange was used in preparation of molybdenum oxide dispersions in MCM-41;[17] the loading via the gas phase for the

* To whom correspondence should be addressed. Phone: +49-208-306 2373. Fax: +49-208-306 2995. E-mail: schueth@mpi-muelheim.mpg.de.

(1) Abe, T.; Tachibana, Y.; Iwamoto, M. *Chem. Commun.* **1995**, 1617.
(2) Iwamoto, M.; Abe, T.; Tachibana, Y. *J. Mol. Catal. A* **2000**, *155*, 143.
(3) Wingen, A.; Anastasievic, N.; Hollnagel, A.; Werner, D.; Schüth, F. *J. Catal.* **2000**, *193*, 248.
(4) Fröba, M.; Köhn, R.; Bouffaud, G.; Richard, O.; van Tendeloo, G. *Chem. Mater.* **1999**, *11*, 2858.
(5) Kloetstra, K.; van Bekkum, H. *Stud. Surf. Sci. Catal.* **1997**, *105*, 431.
(6) Choudhary, V. R.; Jana, S. K.; Kiran, B. P. *J. Catal.* **2000**, *192*, 257.
(7) Zecchina, A.; Scarano, D.; Spoto, G.; Bordiga, S.; Lamberti, C.; Bellussi, G. *Stud. Surf. Sci. Catal.* **1998**, *117*, 343.
(8) Kloetstra, K. R.; van Lauren, M.; van Bekkum, H. *J. Chem. Soc., Faraday Trans.* **1997**, *93*, 1211.
(9) Mehnert, C. P.; Weaver, D. W.; Ying, J. Y. *J. Am. Chem. Soc.* **1998**, *120*, 12289.
(10) Zheng, S.; Gao, L.; Zhang, Q. H.; Guo, J. K. *J. Mater. Chem.* **2000**, *10*, 723.
(11) Morey, M. S.; Stucky, G. D.; Schwarz, S.; Fröba, M. *J. Phys. Chem. B* **1999**, *103*, 2037.
(12) Nagl, I.; Widenmeyer, M.; Grasser, S.; Kohler, K.; Anwander, R. *J. Am. Chem. Soc.* **2000**, *122*, 1544.
(13) Anwander, R.; Gorlitzer, H. W.; Gerstberger, G.; Palm, C.; Runte, O.; Spiegler, M. *J. Chem. Soc., Dalton Trans.* **1999**, 3611.
(14) Gerstberger, G.; Palm, C.; Anwander, R. *Chem. Eur. J.* **1999**, *5*, 997.
(15) Anwander, R.; Runte, O.; Eppinger, J.; Gerstberger, G.; Herdtweck, E.; Spiegler, M. *J. Chem. Soc., Dalton Trans.* **1998**, 847.
(16) Anwander, R.; Roesky, R. *J. Chem. Soc., Dalton Trans.* **1997**, 137.

10.1021/cm0111377 CCC: $22.00
Published on Web 12/20/2001

preparation of vanadium oxide dispersions in MCM-48 is discussed in ref 18.

In this paper we investigate the properties of Y_2O_3/Eu (YOX) dispersions in the ordered mesoporous material SBA-15, for which we propose the name YOX@SBA-15. YOX as bulk material is a well-known red-emitting phosphor, whose structural features and optical behavior have been studied in detail.[19] By highly dispersing the YOX it was hoped to reduce the sensitivity of the luminescence quantum efficiency to impurities by isolation of luminescent centers in very small particles being—on average—impurity-free. In addition, other rare earth metal oxides in high dispersion could be interesting in several catalytic processes. As we also have successfully investigated the loading of ordered mesoporous silica with other rare earth metal oxides, the method to obtain highly dispersed YOX seems to be a generally applicable technique for the preparation of highly dispersed rare earth metal oxides.

Experimental Section

(a) Materials. SBA-15 materials were synthesized with the block copolymer Pluronic P123 (BASF) following published procedures[20] without the aging step at elevated temperature. After synthesis and template removal by calcination at 773 K, the samples were impregnated with aqueous rare earth nitrate solutions of various concentrations via the incipient wetness technique. In most experiments, a mixture of europium and yttrium nitrate (97 atom % Y, 3 atom % Eu) was used. Additionally, erbium oxide doped samples were synthesized using aqueous erbium nitrate solution and europium oxide doped samples were prepared with europium nitrate as precursor. After impregnation and drying at 363 K, the samples were calcined at 873 K for 1 h with a 2 K/min heating ramp to the final temperature. For some samples the procedure of impregnating, drying, and calcination was repeated to obtain higher loadings. All samples were stored above KOH to prevent sorption of water or CO_2 from the atmosphere.

(b) Characterization. Low angle X-ray diffraction patterns were recorded with a Stoe STADI P diffractometer in the Bragg−Brentano (reflection) geometry. The step width was 0.01° at an acquisition time of 40 s per step. Midangle patterns were recorded with the same instrument, but with a step width of 0.1° and an acquisition time of 600 s per step, or with a Stoe STADI P diffractometer in the Debye−Scherrer (transmission) geometry equipped with an area sensitive detector. Here the step width was 2.5° at an acquisition time of 480 s per 2.5°.

Nitrogen sorption isotherms were measured at liquid-nitrogen temperature with an ASAP 2010 adsorption analyzer from Micromeritics. Before the measurement the calcined samples were vacuum-outgassed for at least 4 h at the temperature 473 K. Surface areas were obtained from BET treatment of the isotherms in the range of relative pressures 0.05−0.25. No capillary condensation took place in that range, so that the results are not influenced by this effect. However, there is evidence that SBA-15 contains micropores, which means that the BET surface areas cannot be taken at face value but only as a comparison in a series of samples.

TEM images were obtained with a HF 2000 microscope from Hitachi equipped with a cold field emission gun. The acceleration voltage was 200 kV. For EDX measurements, carried out during the TEM investigations, an electron beam was focused to a spot approximately 8 nm in diameter.

Optical investigations were carried out on a home-built spectrometer, the exact construction of which is described in ref 21.

IR spectra were recorded with a SpectraTec Research Plan microscope, which was coupled with an IR spectrometer type Magna 550 from Nicolet. Samples were placed in a specially designed cell[22] and outgassed in a vacuum before the measurement at 473 K overnight.

Results and Discussion

(a) TEM. In general, the TEM of the unloaded and the loaded SBA-15 samples shows well developed hexagonal structures, if viewed along the channel axis, and parallel lines, if viewed in the perpendicular orientation. This is the normal pattern observed for a well ordered SBA-15 structure. The contrast between the wall and the pores of the rare earth loaded samples was consistently higher than that for all silica materials if viewed along the channel axis, and in most cases no separate dark spots, which would be indicative of rare earth oxide particles, can be detected. This is a first hint that the rare earth oxide is coating the structure rather than present as small oxide particles.

On closer inspection of the TEM images with viewing direction parallel to the channel axis, dark edges at the silica walls of YOX@SBA-15 are visible (Figure 1b) in many regions. They are probably caused by a rare earth oxide layer, deposited fairly homogeneously on the host structure. An artifact brought about by an unfortunate focus condition can be excluded, as this dark lining is visible for a wide range of different focus conditions. At some places, especially for more highly loaded samples, blocking of the channel system, probably by YOX particles, is additionally visible (Figure 1c).

TEM pictures with the viewing direction perpendicular to the channel axis show thicker walls and a lower contrast between channel walls and the inner region of pores for the loaded samples (Figure 2). The phenomenon of a lower contrast seems to be counterintuitive for materials loaded with a denser oxide. However, it can be rationalized, if one considers the path of the electrons through the material more carefully: The parallel lines do not correspond to a lamellar material but to a first approximation result from the projection of a bundle of tubes. So even for the brighter sections in the TEM the electron beam passes partly through matter, while for the dark sections more matter is present in the beam, since it passes not perpendicularly through the wall but under an angle of 30°. A simple geometrical calculation (see inset in Figure 2) shows that for small wall thicknesses the path length for the electron grows with the wall thickness d for the beam passing perpendicularly through the wall (trace 1) and with $4d$ for the beam passing roughly parallel to the wall (trace 2). The ratio between the two thus initially remains constant. However, as soon as the limiting situation is reached in which beam 2 passes only through matter (dark shaded parts in the figure), with increasing wall thickness there is no more effect on trace

(17) Wong, S. T.; Lin, H. P.; Mou, C. Y. *Appl. Catal. A* **2000**, *198*, 103.
(18) van der Voort, P.; Morey, M.; Stucky, G. D.; Mathieu, M.; Vansant, E. F. *J. Phys. Chem. B* **1998**, *102*, 585.
(19) Blasse, G.; Grabmaier, G. B. *Luminescent Materials*; Springer-Verlag: Berlin−Heidelberg−New York, 1994
(20) Zhao, D. Y.; Feng, J. L.; Huo, Q. S.; Melosh, N.; Fredrickson, G. H.; Chmelka, B. F.; Stucky, G. D. *Science* **1998**, *279*, 548.
(21) Ihlein, G. Thesis. Johann Wolfgang Goethe Universität: Frankfurt am Main, 1998.
(22) Schüth, F.; Demuth, D.; Zibrowius, B.; Kornatowski, J.; Finger, G. *J. Am. Chem. Soc.* **1994**, *116*, 1090.

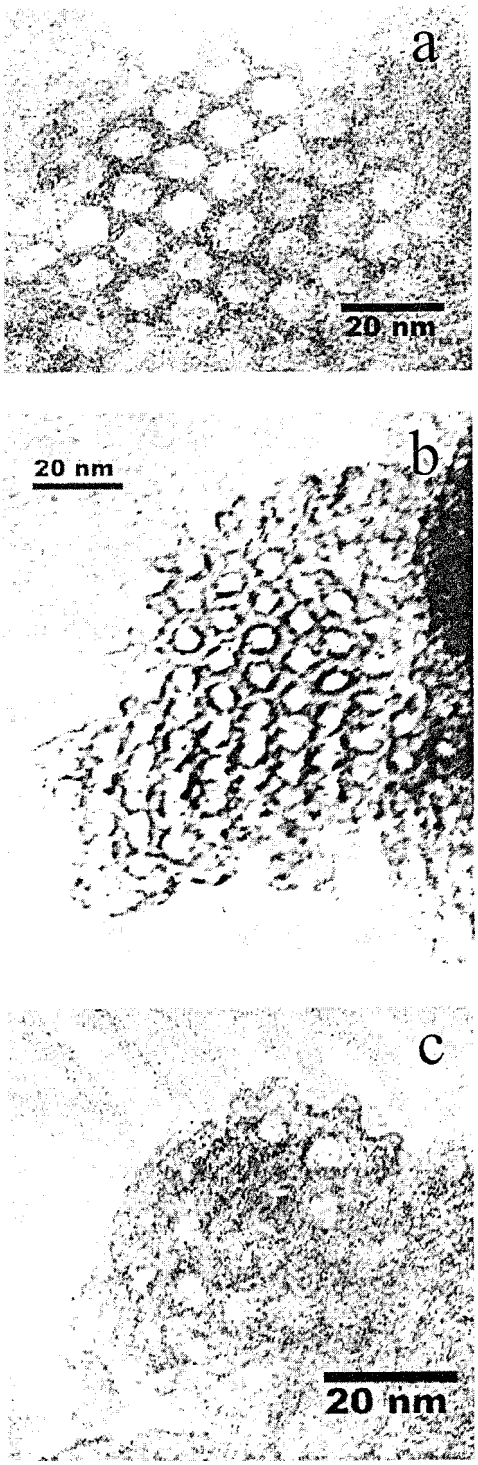

Figure 1. TEM images of SBA-15 (a) and YOX@SBA-15 (b and c). The YOX content is 28 wt %, and the viewing direction is parallel to the channel axis. In part b the coating is visible as the high contrast feature; in part c partly clogged pores can be seen.

2, but trace 1 still is further attenuated, which leads to decreasing contrast. A related line of argument can be put forward for the other major orientation where lines would be visible, that is, the viewing direction along (110). A similar effect, although in a somewhat more complicated manner, arises, if a wall exceeding a certain thickness is covered by a higher scattering and absorbing material. Such an effect and the corresponding TEM spectra could principally be modeled. However, because

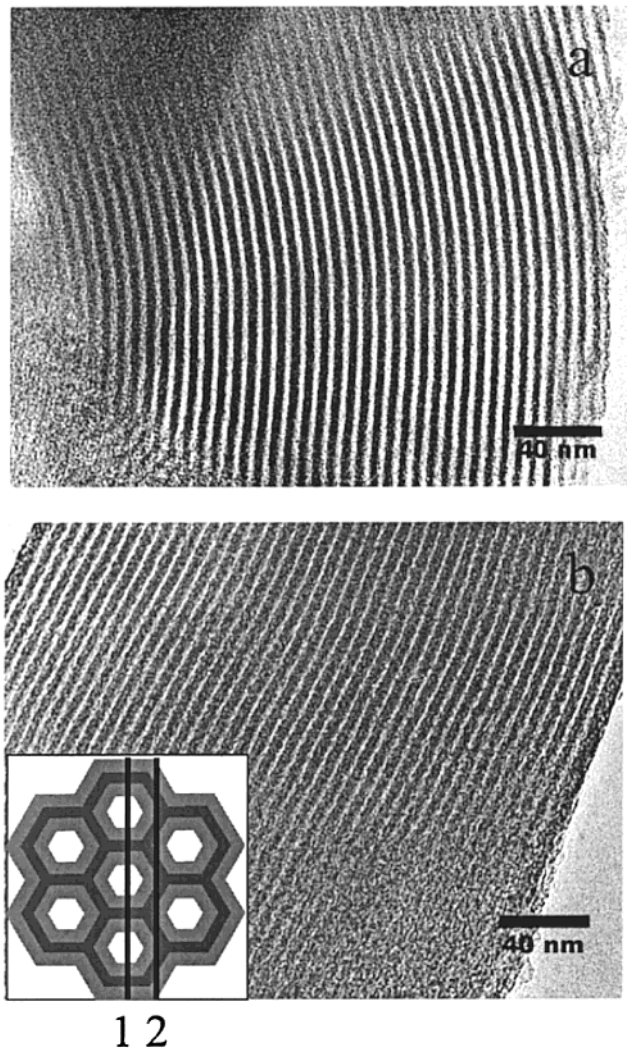

Figure 2. TEM images of SBA-15 (a) and YOX@SBA-15 (b) with a YOX content of 28 wt %. The viewing direction is perpendicular to the channel axis. The inset in part b illustrates why the contrast is lower in the loaded sample (for explanation, see text).

of the imperfection of the structure (deviation from hexagonal cells, faults, inhomogeneous coating), no good match between experimental and calculated data can be expected, which is the reason such detailed modeling was not attempted.

Spot EDX measurements with a resolution of about 8 nm were also carried out during the TEM investigations. They reveal a homogeneous distribution of rare earth oxide in the host material. For samples only doped once, no pure rare earth oxide particles could be found with this technique, neither inside the host material nor on the external surface or as separate particles. This observation again supports the hypothesis that the rare earth oxide covers the internal surface of the SBA-15.

(b) N_2-Sorption. The sorption isotherm of the parent SBA-15 corresponds to isotherms found in the literature. The rare earth oxide loaded samples retain the same shape of the isotherm; however, the amount adsorbed is lowered and the onset of the capillary condensation step is shifted to lower relative pressures (Figure 3). The hysteresis loop is not substantially widened. Such a widening could be expected for an incorporation of small, isolated particles in the channel system of the host

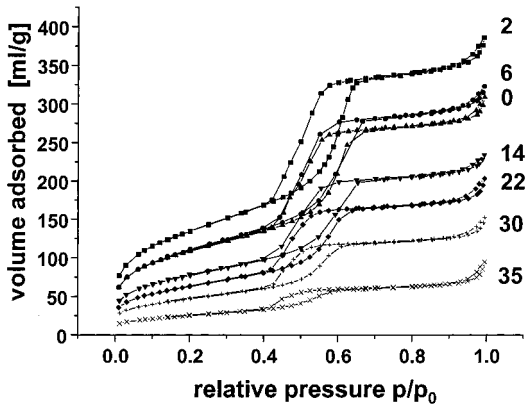

Figure 3. Exemplary series of N_2-sorption isotherms of YOX@SBA-15 samples with different rare earth contents (given in the figure as wt %). As described in the text, for low loading quite often higher volumes adsorbed and higher BET surface areas were observed than those for the parent sample.

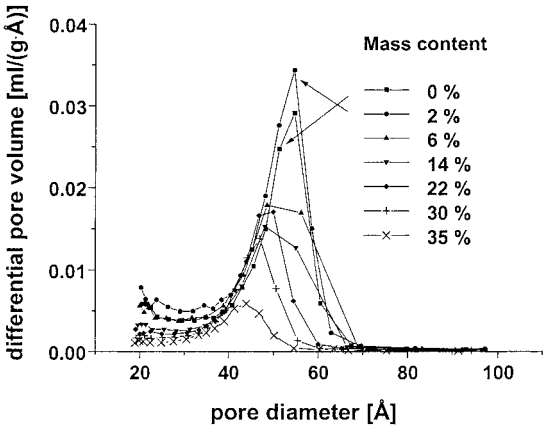

Figure 4. Pore size distributions calculated from the adsorption branch of the isotherms given in Figure 3 using the BJH algorithm.

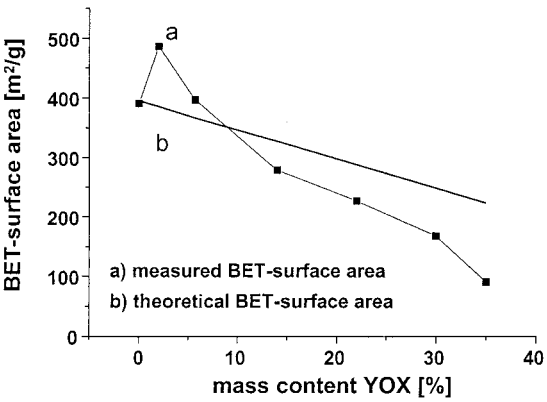

Figure 5. Typical dependence of BET surface area on the loading for YOX@SBA-15 loaded with different amounts of YOX. The line gives the theoretical curve calculated using eq 1.

structure, since this would lead to closed-off voids in the channel system and thus to the so-called ink bottle effect.[23] For the very low loadings, sometimes actually a higher total volume of nitrogen was adsorbed than that for the parent sample. Such loading experiments were performed for many samples, and the scatter in the data for different samples was up to 15% for the total volume adsorbed and the BET surface area. Especially for low loading levels, though, the volume adsorbed and the BET surface area were in several cases higher than those for the parent material. This effect was observed so frequently that—even taking into account the high data scatter—there seems to be an underlying physical reason for this. It has recently been pointed out that block polymer templated ordered mesoporous materials can have micropores in the walls or at least a very rough channel surface.[24−26] In ref 24 the structure of the SBA-15 walls was carefully investigated by sorption, TEM, XRD, and modeling of the XRD patterns. The authors found that, for a material which had been prepared without an additional treatment of the initally formed SBA-15 at elevated temperature in the mother liquor, the walls had a "microporous corona" resulting from partial embedding of the PEO part of the surfactant in the walls. The authors suggest that an additional treatment at elevated temperatures leads to expulsion of the PEO chains and restructuring of the walls. Our parent materials had been synthesized without the additional treatment at elevated temperatures, and thus had the microporous corona. It would be expected that such a low density, microporous silica coating of the walls is a rather unstable situation. It seems thus feasible that an additional step in solution, such as the loading with yttria, can change this microporous corona in a difficult-to-control manner and lead to scatter in the sorption data at low loading. Even an increase in specific surface area and volume adsorbed seems possible, if restructuring in that part of the walls takes place. However, our data are not sufficient to prove these ideas and additional work is necessary to substantiate these suggestions.

The shift of both branches of the sorption isotherms is not as clearly seen in the isotherms themselves but in the corresponding BJH plots. The BJH treatment correlates the pressure of capillary condensation with corresponding pore sizes and thus makes it easier to detect small changes. A BJH plot derived from the adsorption branch of the hysteresis is given in Figure 4, where the constant decrease of the pore diameter with an increasing rare earth oxide content is clearly visible. The adsorption branch was chosen for this analysis, because the hysteresis loop closes at around $p/p_0 = 0.42$, so that network percolation effects on the desorption branch cannot fully be excluded. However, a similar shift is seen for the pore size distribution evaluated from the desorption branch.

The specific surface area is decreasing with increasing rare earth content. Measured BET surface areas for samples with different rare earth contents are given in Figure 5. As explained above, the scatter in the volumes adsorbed and the BET surface areas could amount to about 15%, if samples were resynthesized. Total collapse of the structure at high yttria loadings exceeding approximately 25 wt % was observed, if MCM-41 or SBA-15 samples with thinner pore walls were used as

(23) See, for instance: Gregg, S. J.; Sing, K. S. W. *Adsorption, Surface Area and Porosity*; Academic Press: London, 1982. Rouquerol, F.; Rouquerol, J.; Sing, K. S. W. *Adsorption by Powders and Porous Solids*; Academic Press: San Diego, 1999.

(24) Imperor-Clerc, M.; Davidson, P.; Davidson, A. *J. Am. Chem. Soc.* **2000**, *122*, 11925.

(25) Göltner, C. G.; Smarsly, B.; Berton, B.; Antonietti, M. *Chem. Mater.* **2001**, *13*, 1617.

(26) Joo, S. H.; Choi, S. J.; Oh, I.; Kwak, J.; Liu, Z.; Terasaki, O.; Ryoo, R. *Nature* **2001**, *412*, 169.

the starting materials. The stability of such material is obviously not sufficient to accommodate the local structural changes brought about by the rare earth oxide introduction.

The almost straight line represents the decrease of the specific surface area calculated under the assumption of a homogeneous coating of SBA-15 with rare earth oxide. Here the influence of an increased mass of the composite materials on the specific surface area and the reduction of the pore diameter was taken into account. The formula used for the calculation is as follows:

$$f_2 = f_1 \frac{m_1}{m_1 + m_2} \frac{\sqrt{r^2 - m_2/(\rho\pi\, l)}}{r} \qquad (1)$$

f_1 is the specific area of the undoped material, m_1 is its mass, m_2 is the mass of the rare earth oxide, r is the pore radius of the undoped material, ρ is the specific density of the rare earth oxide layer, and l is the complete channel length of the channel system of the host material. The length l was determined from the pore size and surface area of the host material by assuming the origin of the total surface area as the inner surface of a cylinder with a mean diameter obtained by the BJH calculation.

As discussed above, the measured specific surface areas sometimes increase at a low rare earth content. With a further increase of the loading, the surface areas then decrease almost linearly, but somewhat faster than the calculated curve. At high contents exceeding about 35%, a further drop of the surface area is observed. Although not perfect, the correlation between the experimental and the calculated curves can be taken as a further indication of the buildup of a fairly homogeneous coating of the SBA-15 channels with a rare earth oxide layer. The deviations between the observed decrease of the specific surface area and the calculated curve can be explained by several factors, some of them connected with the material itself and some systematic errors in the analysis. First of all, for submonolayer coverage, deviations are expected anyway. Equation 1 assumes a continuous buildup of the layer, but the layer can only form in discrete steps. For submonolayer coverages the surface has to be patchy to some extent, and thus the equation will only approximate the development of surface area with coverage. In addition, some inhomogeneity of the deposition process, which could lead to a partially blocked pore system, and changes of the parent material during the loading process are the factors attributed to the materials themselves. As stated above, this effect was most dramatic for high loadings on MCM-41 or SBA-15 with thinner walls. The specific surface areas of such samples were reduced to some 10 m^2/g, and the low angle X-ray diffraction features were almost completely lost. Systematic errors might lie in the fact that the BET algorithm becomes more and more unreliable with decreasing pore sizes, because multilayer adsorption is suppressed This effect leads to underestimation of the actual surface area and can amount to more than 10%, depending on the actual pore size. Other systematic errors can result from the fact that in eq 1 used for the calculation of the theoretical surface areas of doped samples only the inner surface is taken into account. Furthermore, the density of the rare earth oxide layer was assumed to be identical to that of the bulk material (5.02 g/cm^3), although it might actually be lower or even depend on the thickness of the layer deposited, because of effects of disorder. Considering all these effects, the agreement between the theoretical and the experimental decreases of the surface area is satisfactory.

The monolayer formation is theoretically complete at a rare earth content between 25 and 45 wt % for the host material with a surface area of 390 m^2/g (used in the series of experiments represented in Figure 5), depending on the model assumed for the yttria layer. This consideration fits well the experimental data, at least for a higher rare earth content than about 30 wt %, where a drop in the specific surface area is observed, indicating blocking of part of the pore system by particles formed in the pores at loadings exceeding monolayer coverage.

(c) XRD. The X-ray diffraction pattern is dominated by the low angle reflections below 5° (2θ). No reflections are visible in the wide angle region for materials doped only once, which suggests that the supported rare earth oxide is X-ray amorphous or present in such small particles that it cannot be detected with XRD. Doping samples more than once leads to visible XRD reflections of cubic yttria in the wide angle range. The size of these particles estimated from the Scherrer equation is bigger than the pore diameter and lies at approximately 18 nm. These particles are thus most probably located outside of the pore system of the host structure. This was confirmed by TEM/EDX investigations of samples doped two or three times. In these experiments separate high contrast particles were visible, for which a very high Y/Si ratio above 10 was determined, suggesting that these particles consist of pure yttria.

In the small angle region three reflections with the usually observed intensity ratios are detected for the undoped material (Figure 6a). Doping the samples lowers the intensity of all reflections. This might be due to a disturbed host structure but is more probably caused by a higher absorption factor of rare earth ions for X-rays. Also the intensity ratios between the higher order reflections and the (100) reflection decrease. The diffraction pattern of the unmodified material shows the (110) and (200) reflections in low intensity. A moderate loading leads to the disappearance of these two higher indexed reflections. A very high loading results in the reappearance of the (110) reflection, which now has a much higher intensity than that observed for the unmodified material. Additionally, the (210) reflection becomes visible.

The changes in the intensity ratios between the different reflections can be understood qualitatively, although, further below, a more detailed explanation will be given. In general, the intensity of the higher indexed reflection is influenced by the sharpness of the distribution of electron density in a unit cell; that is, the sharper the electron density function, the higher the intensities. This effect can be observed in common crystal structures, where a high-temperature factor of scattering centers (“smearing out” of the electron density) leads to reduced intensities of higher indexed reflections. If one plots the electron density for the semiamorphous material SBA-15 against the distance

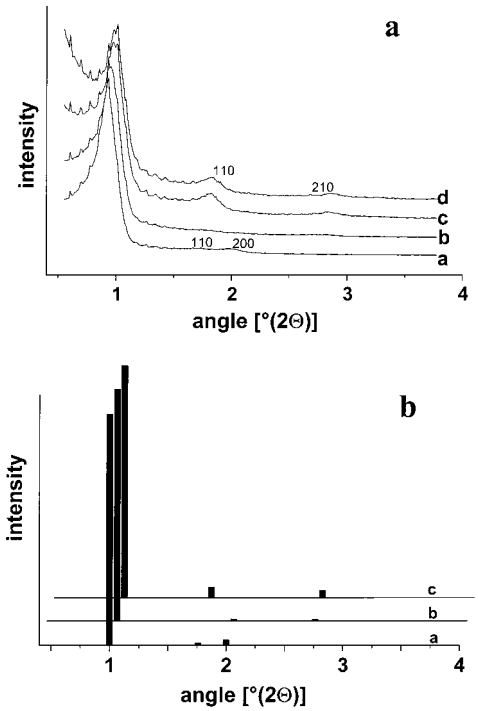

Figure 6. (a) Small angle XRD pattern of SBA-15 (trace a) and YOX@SBA-15 doped once, 37 wt % (trace b), twice, 59 wt % (trace c), and three times, 67 wt % (trace d). (b) Calculated relative intensity of the first four reflections for the unmodified material (a), SBA-15 with a partial coating of 30% (b), and SBA-15 with a monolayer coating of the channel walls (c); see text. Traces b and c in the bottom part of the figure are shifted on the angle scale for clarity.

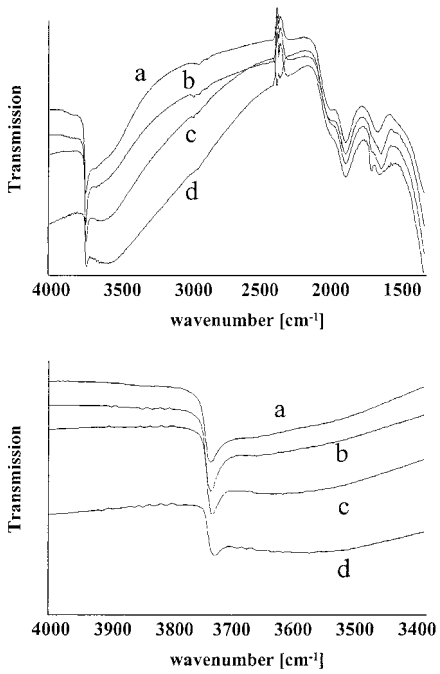

Figure 7. IR spectra between 4000 and 1500 cm^{-1} (a, top) and of the OH region (b, bottom) of YOX@SBA-15 with different contents of YOX. Traces: (a) parent sample; (b) 6 wt % YOX; (c) 22 wt % YOX; (d) 35 wt % YOX.

from the center of a pore, at a certain distance the pore wall is reached. Depending on how well the pore wall is defined, this leads to a more or less steep increase in electron density. The steeper this increase is, the higher is the expected intensity of higher indexed reflections.

X-ray reflections contain the information from coherently scattering domains. Averaged over a scattering domain, a partial coating would result in a flattening of the electron density distribution. The result is a decrease of the intensities of the higher order reflections, which in the case of the low loading samples investigated in this work leads to total vanishing of higher indexed reflections for relatively low loading.

With a higher loading, achieved by doping samples more than once, the partial coating of the low loaded samples is completed, resulting in formation of at least a monolayer of yttria. The electron density distribution is then changed; that is, on the transition from the center of a pore to the SiO_2 wall, the electron density function goes through a maximum in the yttria monolayer. This could lead to the observed, completely different diffraction pattern.

To support this rather qualitative line of argument, a model was developed by which the different kinds of coatings could be simulated and the corresponding diffraction patterns could be calculated from scattering theory. The detailed description of the model goes beyond the scope of this paper, and it will be published elsewhere. Roughly, first an electron distribution for the unit cell is created using a random placing of atoms in predefined sections of the unit cell with probabilities depending on the desired electron density distribution. Then, for this unit cell the diffraction patterns are calculated. Using this procedure, any situation between a purely siliceous material and coatings of various density and thickness can be modeled in a consistent way.

A comparison of diffraction patterns calculated with this model (Figure 6b) with the measured patterns shows that the pattern of the highly doped material corresponds to a completely yttria coated silica wall with a yttria layer thickness of about 0.4 nm. The simulation for a partially coated structure shows a significant loss of intensity of the higher indexed reflections. Using the model discussed above, it was possible to simulate all changes of the diffraction patterns with increasing loading almost quantitatively. The deviations between model and experiment with respect to loading level, which were observed, can be attributed to the difficulties in determining the loading at which full homogeneous monolayer coverage is achieved experimentally and to the fact that at high loadings, approaching monolayer capacity, formation of particles already occurs in part of the structure.

(d) IR. IR measurements reveal a decrease of the silanol band at 3734 cm^{-1} and an increase of a broad absorption band at 3538 cm^{-1} (Figure 7). Remaining silanol groups even at a rare earth content of 35 wt %, where coverage of the silica host should be almost complete, might be explained either by uncondensed silanol groups inside the silica walls or by undoped or less doped regions in the host structure, where silanol groups are still present on the silica walls.

The broad absorption band at 3538 cm^{-1} could result from bridge bonded OH groups in the yttrium oxide adlayer or could result from adsorbed water, which is a way to lower the surface energy.

(e) Optical Spectra. Optical excitation and emission spectra are shown in Figures 8 and 9. In comparison

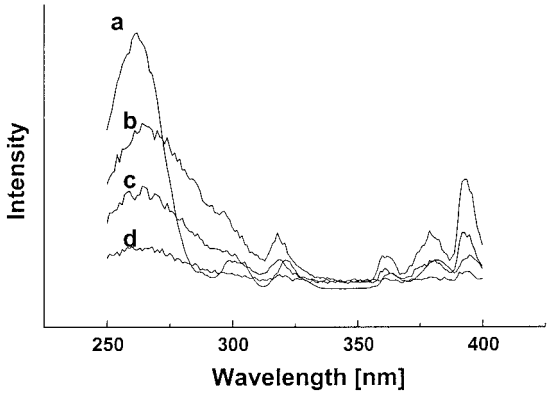

Figure 8. Excitation spectra of bulk YOX (a) and YOX@SBA-15 with 35 wt % YOX (b), 22 wt % YOX (c), and 6 wt % YOX (d). The spectrum of bulk YOX is scaled down by a factor of 14.

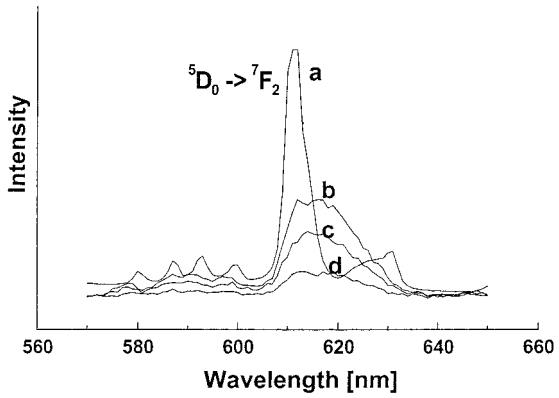

Figure 9. Emission spectra of bulk YOX (a) and YOX@SBA-15 with 35 wt % YOX (b), 22 wt % YOX (c), and 6 wt % YOX (d). The spectrum of bulk YOX is scaled down by a factor of 14.

with the case of the bulk material, the excitation band, which is due to a charge transfer transition, is broadened. This is expected for an amorphous material with varying bond lengths, which result in different excitation energies. Emission bands are broadened probably for the same reason. Quantum yields of all composite materials are below 10% and therefore one magnitude lower than the quantum yield of the bulk material. This can be due to different effects. First, the lattice of the YOX surface layer will be less rigid than that for bulk YOX, which can lead to increased thermal quenching. In addition, the IR spectra revealed substantial intensity in the OH absorption region between 3000 and 4000 cm^{-1}, which can be attributed to bridge bonded OH groups, most probably located in the framework. These OH groups can lead to vibrational deexcitation, to which Eu^{3+} is highly susceptible.

Final Discussion and Conclusions

The experimental data confirm a very high dispersion of rare earth oxides in the ordered mesoporous host material SBA-15 up to loadings exceeding 30 wt %. TEM images, N_2-sorption measurements, XRD, and IR measurements all support the hypothesis of a coating of the host surface with a thin layer of rare earth oxide. One might also think about supporting the notion of a coating by PZC (point of zero charge) measurements, since the PZC values of silica and yttria are substantially different. Such experiments have been performed for the materials produced here, and for the loaded materials indeed a PZC close to the one reported for pure yttria was measured. However, PZC values are determined via mobility measurements in an electric field and thus give information on the external particle surface properties only. Whether or not the channel walls are coated with another material will not be revealed by PZC analysis, and therefore the results were not reported and discussed in detail above.

Spreading of oxides on other oxide surfaces is a well-known effect and exploited technically, for instance, in the SCR catalyst for the reduction of NO_x with ammonia in power plants. This catalyst consists primarily of a titania support, on which vanadia, among others, is supported as the active phase and spreads to a monolayer.[27] Whether an oxide spreads or not is dependent on the surface energies of the participating species. If there is an energetically favorable interaction between the support and the spread oxide, a monolayer will form. At coverages exceeding the monolayer, the supported oxide will behave in the regular way; that is, particles will form, since the surface interaction does not extend beyond the monolayer to an appreciable extent. Whether spreading for a particular combination of materials occurs or not is difficult to predict. One indication for spreading is the fact that mixed oxides of the support and the spread oxide are stable. This is the case for silica and rare earth elements, where many different rare earth silicates have been reported. Accordingly, the coating of silica materials by lanthanum oxide has been described earlier.[28] Also, for instance, for alumina as support the spreading of rare earth oxides is a known phenomenon.[29,30] As the behavior of lanthanum compounds is rather similar to that of other rare earth compounds, the same behavior can be expected for most other rare earth oxides. From hindsight, it thus does not seem to be too surprising that not only conventional silicas can be coated with a monolayer of rare earth oxides, but also ordered mesoporous silica.

Since rare earth oxides have interesting catalytic properties for many catalytic reactions, among others for the activation of hydrocarbons at higher temperatures, these materials could be interesting for catalytic applications. For many such reactions, higher surface areas, which are difficult to obtain for pure rare earth oxides, could be advantageous. Supporting such oxides on high surface area silicas could be an interesting method to obtain materials with the surface area of ordered mesoporous silicas but with the surface functionality of the corresponding rare earth oxide. Investigations directed to the use of such composites as catalysts are under way. In addition, although the optical properties of the materials studied in this report are disappointing, other rare earth oxides could have more interesting properties.

(27) For instance: Bond, G. C.; Flamerz Tahir, S. *Appl. Catal.* **1991**, *1*, 1.
(28) Tan, Y. S.; Lin-Qi, D.; Da-Shun, L.; Dong, W. *J. Catal.* **1991**, *129*, 447.
(29) Bettmann, M.; Chase, R. E.; Otto, K.; Weber, W. H. *J. Catal.* **1989**, *117*, 447.
(30) Scheithauer, M.; Knözinger, H.; Vannice, M. A. *J. Catal.* **1998**, *178*, 701.

Summarizing, we demonstrated that it is possible to obtain rare earth metal oxides in very high dispersion by supporting them on the ordered mesoporous silica SBA-15. All analytical methods suggest that the rare earth oxides spread to form a monolayer. Only after completion of the monolayer do nanoparticles form in coexistence with the monolayer. The approach seems to be rather versatile and will probably work for most of the rare earth oxides and mixtures of them, which gives access to a wide range of materials with different surface properties.

Acknowledgment. In addition to the funding by the Max-Planck Society, this study was funded by the DFG under Grant Number Schu744/8-2, and both are gratefully acknowledged.

CM0111377